

Neutrino-driven supernovae:

An accretion instability in a nuclear physics controlled environment

H.-T. Janka^{a*}, R. Buras^a, F.S. Kitaura Joyanes^a, A. Marek^a, M. Rampp^a, and L. Scheck^a

^aMax-Planck-Institut für Astrophysik,
Karl-Schwarzschild-Str. 1, D-85741 Garching, Germany

New simulations demonstrate that low-mode, nonradial hydrodynamic instabilities of the accretion shock help starting hot-bubble convection in supernovae and thus support explosions by the neutrino-heating mechanism. The prevailing conditions depend on the high-density equation of state which governs stellar core collapse, core bounce, and neutron star formation. Tests of this sensitivity to nuclear physics variations are shown for spherically symmetric models. Implications of current explosion models for r-process nucleosynthesis are addressed.

1. INTRODUCTION

Supernova (SN) models in spherical symmetry (1D) — even the latest ones with “Boltzmann neutrino (ν) transport” [1] — do not explode, neither by the prompt bounce-shock mechanism, nor by the delayed neutrino-heating mechanism. Suggestions that neutron-finger convection in the neutron star (NS) could enhance the ν luminosity and thus the heating behind the shock [2] could not be confirmed by detailed analysis [3]. Also Ledoux convection in the nascent NS seems to be ineffective in this respect [4, 5]. A reduction of the ν opacity by several 10% at densities below $\sim 10^{13} \text{g cm}^{-3}$ would also allow ν 's to leave the accretion layer more easily and could produce explosions [6], but a physical effect of corresponding size is not known.

Multi-dimensional simulations of core-collapse SNe revealed that hydrodynamic overturn behind the stalled accretion shock develops on a relevant timescale and increases the efficiency of the ν -heating mechanism, enabling explosions even when spherical models fail [7]. Initially there was hope that this new twist in the theory of SNe was the long-sought guarantee for “robust” explosions. But the first generation of multi-dimensional models employed a simplified treatment of the ν transport — at best by grey flux-limited diffusion schemes — which fell much behind the sophistication of the transport in non-exploding 1D models. It was therefore suspected that the transport approximations might have contributed to the success of the multi-dimensional simulations [8].

Recently, two-dimensional (2D) models have become available with a significant improvement of the ν transport by solving the energy-dependent equations of ν number,

*This work was supported by the Sonderforschungsbereich (SFB) 375 “Astro-Particle Physics” and by the SFB-Transregio 7 “Gravitational Wave Astronomy” of the Deutsche Forschungsgemeinschaft.

energy, and momentum, making use of closure relations obtained from a model Boltzmann equation [4, 9]. The description of ν -matter interactions has thus reached a new level of accuracy and refinement, although the transport is still treated to be essentially radial (lateral flux components are ignored in the moments equations but terms associated with lateral velocities and lateral gradients of ν pressure are included). Simulations with thus improved treatment of the ν physics could not find explosions despite of convective activity in the ν -heating layer behind the SN shock [5], confirming the suspicion that radical transport approximations might have favored the rapid and powerful explosions seen in other 2D and 3D models [7, 10].

So what is missing in the currently most advanced SN models which fail to produce explosions? In the following, we shall first briefly summarize the status of core-collapse modeling by the Garching group. In particular, we shall discuss that any limitation of the angular wedge of 2D simulations to less than 180 degrees (e.g. to 90 degrees as in many previous simulations) imposes artificial constraints to the fluid flow and suppresses large-scale modes that can play an important role for the growth of convection. It is further demonstrated that even a “modest” amount of rotation in the SN core, in the ballpark of predictions of current stellar evolution models [11], may have an important impact on the postbounce evolution. Finally, we shall elaborate on uncertain aspects of the nuclear physics which the SN shows sensitivity to.

2. EXPLOSION MODELS

Simulations leading to explosions can be reported for stars near the low-mass end of SN progenitors, namely for stars in the mass range of $\sim 8\text{--}10 M_{\odot}$ with O-Ne-Mg cores [12], and for an $11.2 M_{\odot}$ progenitor [13], both characterized by small cores of less than $\lesssim 1.3 M_{\odot}$ (O-Ne-Mg or Fe, respectively) and a steep density decrease (entropy increase) outside.

2.1. Stars in the 8–10 M_{\odot} range with O-Ne-Mg cores

The main improvement of our new simulations of O-Ne-Mg core collapse — which we did so far only in spherical symmetry — compared to previous approaches is the more accurate, spectral treatment of ν transport and ν -matter interactions. Using the nuclear equation of state (EoS) of Lattimer & Swesty [14] and more recently also that of Hillebrandt & Wolff [15], we could *not* confirm the prompt explosions found in calculations with simpler ν treatment [15]. The shock is created much deeper inside the collapsing core than in the “old” models (cf. also Ref. [16]), typically at a mass coordinate around $\sim 0.45 M_{\odot}$ [17] (defined by the moment when the postshock entropy first exceeds $3 k_B$ per nucleon), and it stalls (defined by the time when the postshock velocity becomes negative) only 1.2 ms later at $\sim 0.8 M_{\odot}$, still well inside the neutrinosphere and *before* energy losses by the prompt ν_e burst could have contributed to its damping [17]. We also do not find the powerful shock revival by ν heating as seen in Ref. [18] and for some choice of the nuclear EoS by Fryer et al. [19]. Instead, the shock continuously expands due to the monotonically decreasing preshock density and the steep density decline at the interface between C-O shell and He shell (Fig. 1). At the end of our simulation the mass accretion rate by the shock has correspondingly dropped to less than $0.03 M_{\odot} \text{ s}^{-1}$. Although our simulation is not yet finally conclusive in this point, we see indications that a ν -driven wind

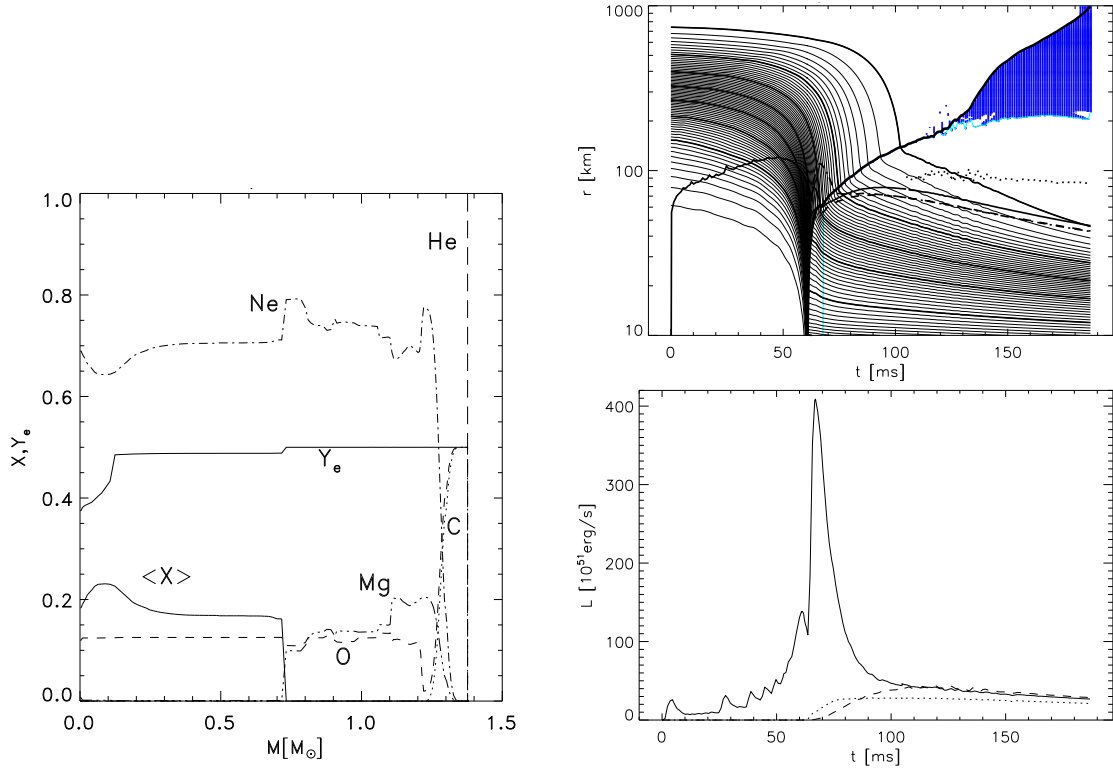


Figure 1. *Left*: Composition in the highly degenerate $1.38 M_{\odot}$ core of an $8\text{--}10 M_{\odot}$ progenitor [12] with O, Ne and Mg in the central region enclosed by a C-O shell. $\langle X \rangle$ denotes the mass fraction of a representative neutron-rich heavy nucleus that appears in nuclear statistical equilibrium, and Y_e is the electron fraction. *Right, top*: Mass trajectories, shock position (thick solid line that rises to the upper right corner of the plot, where it reaches the surface of the C-O shell), neutrinospheres (ν_e : solid; $\bar{\nu}_e$: dash-dotted; ν_{μ} , $\bar{\nu}_{\mu}$, ν_{τ} , $\bar{\nu}_{\tau}$: dashed), and gain radius (dotted) for the collapsing O-Ne-Mg core. The mass trajectories are equidistantly spaced with intervals of $0.02 M_{\odot}$. The outermost line corresponds to an enclosed mass of $1.36 M_{\odot}$ near the outer edge of the carbon shell. The (blue) hatched region is characterized by a dominant mass fraction of alpha particles. *Right, bottom*: Luminosities of ν_e (solid), $\bar{\nu}_e$ (dashed) and heavy-lepton ν 's (individually; dotted) as functions of time. The sawtooth pattern during the collapse phase until about 50 ms is a numerical artifact. (The plots were taken from Ref. [17].)

begins to fill the volume between SN surface and shock and will lead to mass ejection with a rather low explosion energy (a few 10^{50} erg due to the wind power and nuclear burning). Little nickel production ($\sim 0.01 M_{\odot}$), can be expected, corresponding to the wind mass loss rate that can be estimated for an initial $\nu_e + \bar{\nu}_e$ luminosity of $\sim 8 \times 10^{52}$ erg s $^{-1}$ (Fig. 1) using the equations in Refs. [20]. The baryonic mass of the NS will be very close to or only some $0.01 M_{\odot}$ less than the C+O core mass (which is $1.38 M_{\odot}$). These findings are very similar to the outcome of simulations of accretion induced white dwarf collapse to NSs (AICs) [21].

A weak explosion of an $8\text{--}10 M_{\odot}$ star has been suggested as an explanation of the observed properties of the Crab SN remnant [22]. The wind-driven explosion seen in our models, however, does not provide the conditions for the low-entropy, low- Y_e r-process

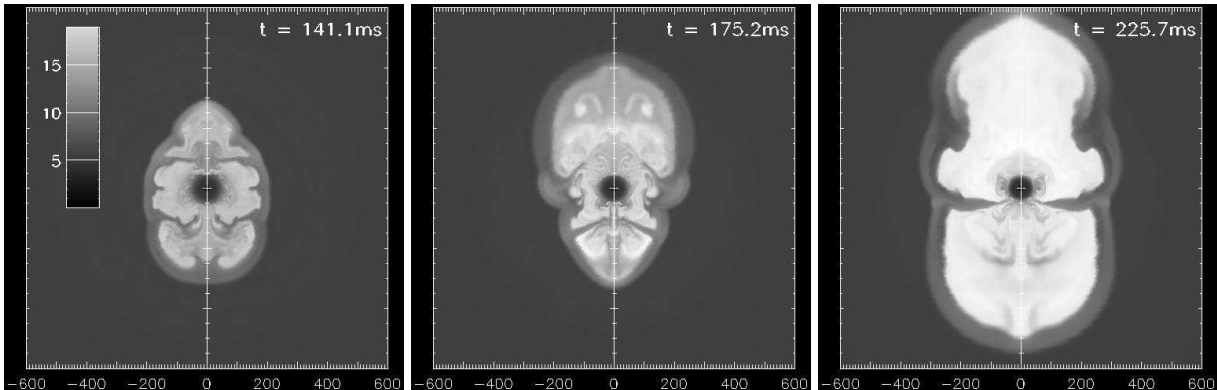


Figure 2. Three stages (at postbounce times of 141.1 ms, 175.2 ms, and 225.7 ms from left to right) during the evolution of a (non-rotating) $11.2 M_{\odot}$ progenitor model from Ref. [13], visualized in terms of the entropy. The scale is in km. The dense NS is visible as low-entropy circle at the center. The computation was performed in spherical coordinates, assuming axial symmetry, and employing the “ray-by-ray plus” variable Eddington factor technique [24] for treating ν transport in multi-dimensional SN simulations. Equatorial symmetry is broken on large scales soon after bounce, and low-mode convection begins to dominate the flow between the NS and the strongly deformed SN shock. The model continues to develop a probably weak explosion, the energy of which was not determined before the simulation had to be stopped because of CPU time limitations.

nucleosynthesis discussed for prompt explosions of collapsing O-Ne-Mg cores in previous work [23]. R-processing in the high-entropy environment of the ν -driven baryonic wind can also not be expected to take place, because sufficiently high entropies, short expansion timescales, and low proton-to-baryon ratios require the NS to be very massive ($\sim 2 M_{\odot}$) and compact ($\lesssim 10$ km) (e.g., Refs. [20]). It is therefore unclear how O-Ne-Mg core collapse events could contribute to the production of high-mass r-process nuclei.

2.2. Massive stars with iron core

Progenitor stars in the mass range between $11 M_{\odot}$ and $25 M_{\odot}$ were found to neither explode by the prompt bounce-shock mechanism nor by the delayed ν -heating mechanism in spherically symmetric simulations [27], in agreement with results of other groups [1]. This implies that state-of-the-art SN models do not support suggestions that r-process nucleosynthesis might occur in prompt explosions of low-mass ($\sim 11 M_{\odot}$) progenitors [28].

We have also started to perform core-collapse simulations for the mentioned stellar mass range in 2D, using a polar coordinate grid and assuming azimuthal symmetry [5, 4]. Because of the energy-dependent treatment of ν transport and ν -matter interactions the requirements of CPU time are substantial, and we were so far able to perform only a handful of such 2D calculations. To limit the need of computer resources we initially constrained the computational volume to a $\sim 90^{\circ}$ wedge (between roughly $+45^{\circ}$ and -45° around the equatorial plane and periodic boundary conditions for nonrotating models and between 0° and 90° with reflecting boundaries for rotating ones), using an angular resolution of $\sim 1.4^{\circ}$. This choice was also motivated by 2D models of the first generation which were able to obtain explosions with a similar setup due to the help of hot-bubble

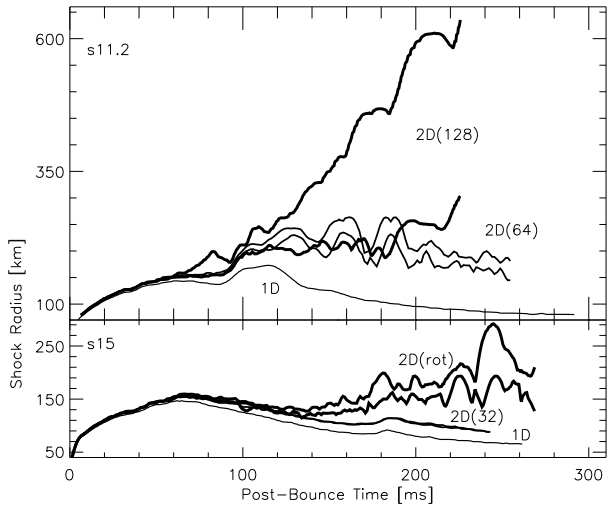


Figure 3. Maximum and minimum radii of the shock (giving a rough measure of deformation) vs. time for 2D simulations with a polar coordinate grid (models “2D”), compared to 1D results with the same physics, but no convection (models “1D”). *Top*: $11.2 M_{\odot}$ star [13], simulated with a full 180° grid (Model 2D(128)) and with a 90° angular wedge around the equatorial plane (Model 2D(64)). *Bottom*: $15 M_{\odot}$ star (Model s15s7b2 of Ref. [25]) without (Model 2D(32)) and with rotation (Model 2D(rot); see also [5, 26]). In the former 2D simulation a 90° wedge around the equator was used, in the latter a 90° grid from pole to equator.

convection [7].

First simulations of stars of 11.2 , 15 , and $20 M_{\odot}$ with a 90° wedge, however, did not produce explosions [5]. This suggests that the success of the previous calculations with simplified transport was most probably connected with the use of transport approximations. One of our new models, a $15 M_{\odot}$ star (Model s15s7b2 of Ref. [25]), was also collapsed with a modest rotation: The pre-collapse core was assumed to rotate (essentially rigidly) with a period of 12 s, i.e. $\Omega \approx 0.5 \text{ rad s}^{-1}$ (see Fig. 1 in [26]), which is significantly faster — but not orders of magnitude faster — than predicted by the latest stellar evolution models [11]. Even this “modest” amount of rotation turned out to make a big difference. As visible in the lower panel of Fig. 3, the shock expands to a much larger radius than in the 2D simulation without rotation (although both simulations did not lead to explosions within ~ 270 ms of postbounce evolution), mostly because of the influence of centrifugal forces and the more violent convection in a more extended region of ν heating [5].

2.3. Nonradial shock instabilities and low-mode postshock convection

While the $11.2 M_{\odot}$ simulation with 90° wedge did not explode (see Fig. 3, upper panel), the same model with a full 180° grid developed a presumably weak explosion (Figs. 2 and 3). Equatorial symmetry is broken on large scales some 10 ms after convective activity in the postshock region has started (at ~ 50 ms p.b.), and low modes ($l = 1, 2$) begin to dominate the flow pattern between NS and shock after about 140 ms p.b., a phenomenon which might be linked to the observed large recoil velocities of young pulsars [29]. The convection becomes significantly more violent than in the 90° simulation where obviously important degrees of freedom were suppressed. This latter fact was emphasized in an interesting paper by Blondin et al. [30], who found a similar development of low-mode asymmetries in the postshock flow and shock oscillations as a consequence of the instability of standing accretion shocks (“SASI”) against non-radial perturbations that are amplified in a “vortical-acoustic feedback cycle” [31].

Blondin et al. considered idealized conditions in their numerical studies, assuming

steady-state mass accretion with a constant rate, a fixed inner boundary radius, a simple ideal-gas EoS, and ignoring ν heating and cooling. We decided to test the effects of ν 's and of the size of the angular wedge (and thus of the possible modes) in a separate set of simulations with a realistic EoS but an approximative treatment of the ν transport (as described in Refs. [29]), which allowed us to save computer time and thus to perform faster calculations with higher resolution, and to run more models. The mass accretion rate was given by the collapse of a $15 M_{\odot}$ progenitor star and the NS was replaced by a gravitating point mass inside a contracting inner boundary that followed the behavior of the shrinking NS in our full-scale SN simulations with detailed transport physics.

With this setup we confirmed that 2D simulations with a 180° grid can yield explosions even if models with 90° wedge do not explode. In these studies, with ν effects switched on or off, we found that ν losses promote the action of the vortical-acoustic cycle by allowing matter to settle on the proto-NS surface. Our results show that corresponding shock deformation produces growing perturbations in the postshock flow which can accelerate the onset of convective overturn even in cases where the infall timescale is initially shorter than the growth timescale of Ledoux convection. We also see that dipolar shock oscillations become more violent in case of a rapid contraction of our inner boundary (mimicing a NS that becomes rapidly more compact due to a soft nuclear EoS), thus releasing gravitational binding energy which partly is converted to turbulent kinetic energy of the postshock flow. In this case $l = 1, 2$ modes begin to dominate faster and the SASI conspires with convective instability to establish favorable conditions for a high efficiency of ν heating behind the shock. Both nonradial instabilities differ characteristically in the way how anisotropies emerge: Convective overturn is driven by the negative entropy gradient in the ν -heated layer, which becomes Rayleigh-Taylor (RT) unstable first on small scales, while the SASI starts from vorticity producing sound wave interactions with the shock and induces dipolar oscillations of the postshock layer before convective activity is initiated and the typical RT mushrooms become visible.

2.4. Nuclear physics sets the stage

Nuclear physics therefore governs not only the collapse phase, where electron captures on nuclei were recently included in a much improved way and were found to determine the position of shock formation and the structure of the layers the shock expands into [32] (also W.R. Hix and G. Martínez-Pinedo, this conference). Nuclear physics and in particular the properties of the nuclear EoS also determine the contraction and size of the nascent NS and thus may influence the growth of nonradial instabilities and anisotropies in the postshock accretion flow during the ν -heating phase.

In fact, differences in the nuclear EoS have interesting consequences for core collapse, bounce conditions, shock formation, and postshock evolution in 1D simulations [33] (for a brief summary, see [27]). Figure 4 shows selected results for three different EoSs (Lattimer & Swesty [14], Shen et al. [34], and Wolff & Hillebrandt [15]). The softest of them (L&S) leads to the highest densities at bounce and the smallest enclosed mass of the shock formation position. Later on the nascent NS contracts most rapidly, forcing the shock to retreat much more quickly than in case of, in particular, the stiff Wolff EoS (Fig. 4, upper middle panel). These differences affect the ν luminosities during the ν_e burst and the postbounce accretion phase (Fig. 4, upper right panel). While for the Wolff EoS the ν_e

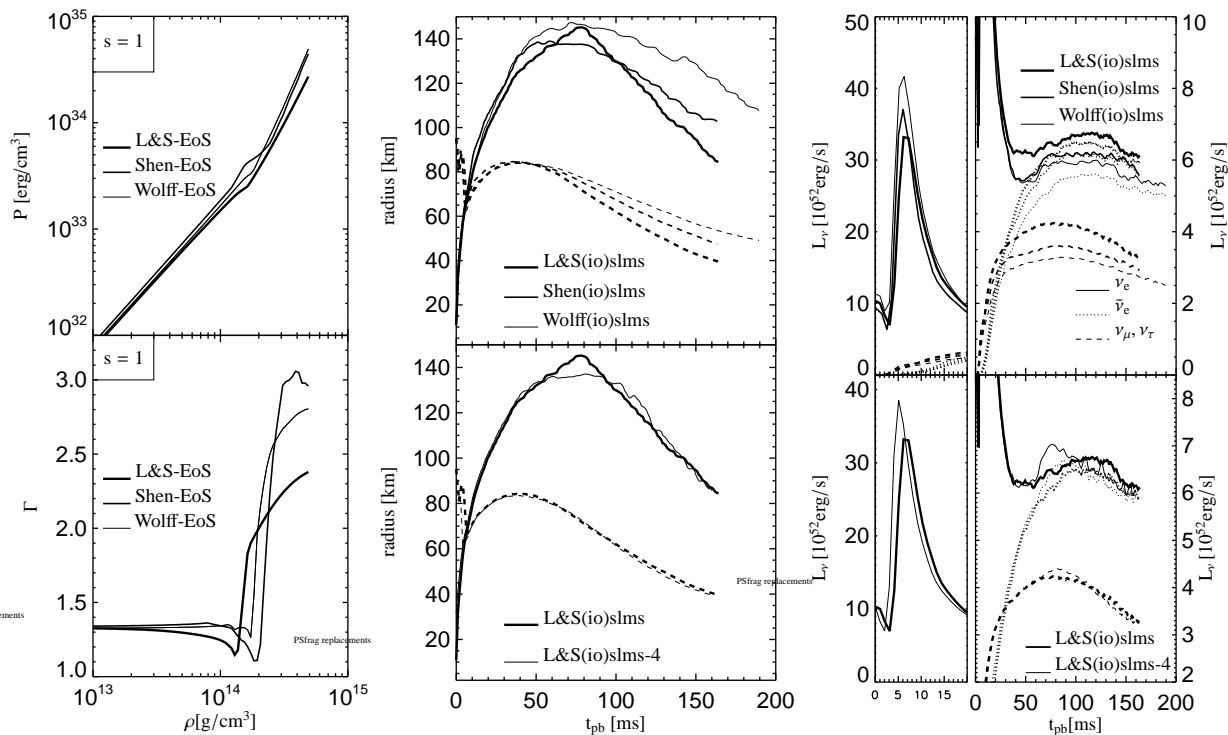


Figure 4. *Left:* Pressure (top) and adiabatic index $\Gamma \equiv (d \ln P / d \ln \rho)_s$ (bottom) vs. mass density for an entropy $s = 1 k_B$ per nucleon (and $Y_e = 0.4$) for the EoSs of Ref. [15] (“Wolff”, thin lines), Ref. [34] (“Shen”, medium) and Ref. [14] (“L&S”, thick). *Middle:* Shock positions (solid lines) and neutrinospheric radii of ν_e (dashed) as functions of time for collapse simulations of a $15 M_\odot$ progenitor (Model s15a28 [13]) with the three nuclear EoSs (top) and with two different EoSs at densities $\rho < 10^{11} \text{ g cm}^{-3}$ (L&S compared to an ideal gas EoS of e^- , e^+ , γ 's, and Boltzmann gases of n , p , α and a representative heavy nucleus in NSE; bottom). *Right:* Prompt ν_e burst (left panel) and postbounce luminosities of ν_e (solid lines), $\bar{\nu}_e$ (dotted) and heavy-lepton ν 's and $\bar{\nu}$'s (dashed) for the simulations of the $15 M_\odot$ star with the three different nuclear EoSs (top) and the two different low-density EoSs (bottom). (The plots were taken from Ref. [33].)

release in the burst is highest, a more compact NS and thus hotter neutrinosphere causes higher post-burst ν luminosities and mean energies. In the lower middle and right panels we show the result of a test which we performed with a four-nuclei NSE-EoS replacing the low-density ($\rho < 10^{11} \text{ g cm}^{-3}$) part of the L&S EoS (where an error in the treatment of α -particles has recently been discovered; C. Fryer, J. Lattimer, personal communication). The conditions in the postshock layer were hardly affected because the gas is disintegrated into free nucleons at the high entropies encountered in simulations with relativistic gravity. Minor differences in the evolution of the shock radius (Fig. 4, lower middle panel) and ν luminosities (Fig. 4, lower right panel) were caused by differences in the mass accretion rate associated with the EoS treatment in the infall region ahead of the shock.

3. SUMMARY

Non-radial instability of the accretion shock can amplify vorticity in the postshock flow and thus can support the growth of convection in the ν -heated layer. It may be an important ingredient for eventually robust explosions by the ν -driven mechanism. Low modes in the flow can develop when the explosion sets in slowly. The relative importance of the different instabilities seems to depend on ν cooling and heating on the one hand and the high-density EoS, which controls the contraction of the nascent NS, on the other. Simulations require the use of a full 180° grid and ultimately may have to be done in 3D.

Acknowledgements. We are grateful to K. Nomoto, A. Heger, S. Woosley, and M. Limongi for providing us with their progenitor data. Supercomputer time at the John von Neumann Institute for Computing in Jülich and the Rechenzentrum Garching is acknowledged.

REFERENCES

1. M. Rampp and H.-T. Janka, ApJ 539 (2000) L33; M. Liebendörfer et al., PRD 63 (2001) 103004, ApJS 150 (2004) 263; T.A. Thompson et al., ApJ 592 (2003) 434.
2. J.R. Wilson and R. Mayle, Phys. Rep. 163 (1988) 63, 227 (1993) 97.
3. S.W. Bruenn et al., ApJ, submitted (astro-ph/0404099).
4. H.-T. Janka et al., in: *Stellar Collapse*, Kluwer, Dordrecht, 2004, p.65 (astro-ph/0212314).
5. R. Buras et al., PRL 90 (2003) 241101.
6. C. Fröhlich et al., ApJ, submitted (astro-ph/0410208).
7. M. Herant et al., ApJ 435 (1994) 339; A. Burrows et al., ApJ 450 (1995) 830; C.L. Fryer, ApJ 522 (1999) 413; C.L. Fryer and A. Heger, ApJ 541 (2000) 1033.
8. A. Mezzacappa et al., ApJ 495 (1998) 911.
9. H.-T. Janka et al., IAU Coll. 192 (astro-ph/0401461).
10. C.L. Fryer and M.S. Warren, ApJ 574 (2002) L65 (2002), ApJ 601 (2004) 391.
11. A. Heger et al., astro-ph/0409422.
12. K. Nomoto, ApJ 277 (1984) 791, ApJ 322 (1987) 206.
13. S.E. Woosley et al., Rev. Mod. Phys. 74 (2002) 1015.
14. J.M. Lattimer and F.D. Swesty, Nucl. Phys. A535 (1991) 331.
15. W. Hillebrandt et al., A&A 133 (1984) 175.
16. E. Baron et al., ApJ 320 (1987) 300.
17. F.S. Kitaura Joyanes, Diploma Thesis, TU München (2003).
18. R. Mayle and J.R. Wilson, ApJ 334 (1988) 909.
19. C. Fryer et al., ApJ 516 (1999) 892.
20. S.E. Woosley, A&AS 97 (1993) 205; Y.-Z. Qian and S.E. Woosley, ApJ 471 (1996) 331; S. Wanajo et al., ApJ 554 (2001) 578; T.A. Thompson et al., ApJ 562 (2001) 887.
21. S.E. Woosley and E. Baron, ApJ 391 (1992) 228.
22. K. Nomoto et al., Nature 229 (1982) 803.
23. J.C. Wheeler et al., ApJ 493 (1998) L101; S. Wanajo et al., ApJ 593 (2003) 968.
24. M. Rampp and H.-Th. Janka, A&A 396 (2002) 361.
25. S.E. Woosley and T.A. Weaver, ApJS 101 (1995) 181.
26. E. Müller et al., ApJ 603 (2004) 221.
27. H.-T. Janka, Proc. 12th Worksh. Nucl. Astrophys., MPA/P14, p. 150 (astro-ph/0405289).
28. K. Sumiyoshi et al., ApJ 562 (2001) 880.
29. L. Scheck et al., PRL 92 (2004) 011103; H.-T. Janka et al., η Car Symp. (astro-ph/0408439).

30. J.M. Blondin et al., ApJ 584 (2003) 971.
31. T. Foglizzo, A&A 392 (2002) 353.
32. K. Langanke et al., PRL 90 (2003) 241102; W.R. Hix et al., PRL 91 (2003) 201102.
33. A. Marek, Diploma Thesis, TU München (2003).
34. H. Shen et al. Nucl. Phys. A637 (1998) 435; Prog. Theor. Phys. 100 (1998) 1013.